## The $\alpha_S$ Dependence of Parton Distributions

A. D. Martin and W. J. Stirling,

Department of Physics, University of Durham, Durham, DH1 3LE, England

and

R. G. Roberts,

Rutherford Appleton Laboratory, Chilton, Didcot, Oxon, OX11 0QX, England.

#### Abstract

We perform next-to-leading order global analyses of deep inelastic and related data for different fixed values of  $\alpha_S(M_Z^2)$ . We present sets of parton distributions for six values of  $\alpha_S$  in the range 0.105 to 0.130. We display the  $(x,Q^2)$  domains with the largest parton uncertainty and we discuss how forthcoming data may be able to improve the determination of the parton densities.

Analysis of the scaling violations of deep inelastic scattering data provides one of the accurate ways to determine the QCD coupling  $\alpha_S$ . The scaling violations observed in recent high precision muon and neutrino deep inelastic data yield values<sup>1</sup> of  $\alpha_S = 0.113 \pm 0.005$  [1] and  $0.111 \pm 0.006$  [2] respectively. Moreover a global parton analysis which includes these data, with other related data, gives  $\alpha_S = 0.113 \pm 0.005$  [3]. However, there are other independent determinations which lie outside this range; for example  $\alpha_S$  determined from LEP event shapes or from  $\tau$  decays. A recent review of all the methods is given by Webber [4] who concludes that the world average is  $0.117 \pm 0.005$ .

 $\alpha_S$  is now also being determined from jet rates observed in the experiments at HERA [5] and Fermilab [6]. These methods have the advantage of determining  $\alpha_S$  over a wide range of  $Q^2$  and it is believed that they will eventually yield values with equal precision to the other determinations of  $\alpha_S$ . However, they require the use of parton distributions which have their own particular value of  $\alpha_S$  and so the question of consistency arises. Does the "output"  $\alpha_S$  depend on the "input" value of  $\alpha_S$ ? In order that the sensitivity to the input partons may be studied, we repeat the global analysis of refs. [3, 7] for various fixed values of  $\alpha_S(M_Z^2)$  in the interval which covers these other independent determinations, namely 0.105 to 0.130. This study allows us to highlight the deep inelastic data that particularly constrain  $\alpha_S$ . Moreover it provides a quantitative estimate of the uncertainty associated with the parton distributions  $f_i(x, Q^2)$  in different regions of x and  $Q^2$ .

An earlier analysis [8], which studied the uncertainty in the determination of  $\alpha_S$ , did provide 4 parton sets which cover a limited range of  $\alpha_S$ . Here we extend the range and use the improved set of deep inelastic and related data. CTEQ [9] have recently presented an additional parton set with a high  $\alpha_S$ , and Vogt [10] has provided 5 sets of GRV [11] partons with  $\alpha_S$  in the interval (0.104, 0.122). The latter is not a global analysis and so cannot accommodate the variation of partons, particularly at larger x, which attempt to compensate for the shift of  $\alpha_S$  from its optimum value.

We base our global next-to-leading analysis on the MRS(A) parametric forms, updated in ref. [7] to include recent HERA data [12, 13]. That is we consider variations about the optimum fit MRS(A')<sup>2</sup>. Fig. 1 shows the  $\chi^2$  values for various subsets of deep inelastic data obtained in six new global fits<sup>3</sup> with different values of  $\alpha_S(M_Z^2)$ . Cross section and asymmetry data for Drell-Yan and W hadroproduction are included in the analysis, but their contributions to  $\chi^2$  are not shown. These data remain well-described in the fits with different  $\alpha_S$  values by slight adjustments of the partonic flavour structure of the proton; they do not pin down  $\alpha_S$ . Also the data for prompt photon production are accommodated as  $\alpha_S$  varies by a change in

Throughout we work in terms of the QCD coupling at the Z pole,  $Q^2 = M_Z^2$ , evaluated in the  $\overline{\rm MS}$  scheme with 5 flavours, which we shall denote simply by  $\alpha_S$ .

 $<sup>^{2}</sup>$ We choose not to base our analysis on the MRS(G) set of partons [7], since this would involve an extra parameter which is only relevant to data at very small x. It therefore would introduce a degree of ambiguity in a domain where the precision of the data is going to rapidly improve. We return to this point later.

<sup>&</sup>lt;sup>3</sup>The six sets have  $\alpha_S = 0.105, 0.110, \dots 0.130$  and are denoted by MRS.105 etc. The parton sets can be obtained by electronic mail from W.J.Stirling@durham.ac.uk.

scale. The  $\chi^2$  profile for the WA70 data is shown in Fig. 1. Only the smallest values of  $\alpha_S$  are disfavoured; the prediction does not fall off quite steeply enough, as the photon transverse momentum increases, to agree with the observed distribution.

The HERA 1993 data [12, 13] are included in the analysis. In addition we show the  $\chi^2$  values for the preliminary 1994 ZEUS data [18] that were obtained with the electron-proton collision point shifted (so that the detectors can gather deep inelastic events at smaller x). Due to the logarithmic scale that has been used for  $\chi^2$  it is easy to be misled by Fig. 1 about the relative importance of various data sets in the determination of  $\alpha_S$ . The  $\chi^2$  profiles at the top of the plot have a more significant impact than those which lie lower down.

Considerable insight into the effect of varying  $\alpha_S$  (and the related ambiguities) can be obtained from Fig. 2. This shows the available data for  $F_2^{ep} = F_2^{\mu p}$  at three particular x values: x = 0.0008 in the HERA range, x = 0.05 which is relevant for W production at Fermilab and x = 0.35 representative of the large x BCDMS precision data which provide the tightest constraints on  $\alpha_S$ . The curves are obtained from the three parton sets which have  $\alpha_S = 0.105, 0.115$  and 0.125. Recall that the optimum overall description occurs for  $\alpha_S = 0.113$  and so the continuous curve gives a better global fit than the ones either side. As expected, the scaling violation is greatest for the partons with the largest value of  $\alpha_S$ . Also, as may perhaps be anticipated, the curves cross in the region of the data, which lie in different intervals of  $Q^2$  for the different values of x. Away from the  $(x, Q^2)$  domain of the data the predictions show a considerable spread. For example for x = 0.0008 and  $Q^2 \sim 10^3 \,\text{GeV}^2$  we see quite a variation in the prediction for  $F_2^{ep}$ . The ambiguity in the small x domain is actually greater than that shown, since the quark sea and the gluon have been constrained to have the same small x behaviour, that is

$$xS \sim A_S x^{-\lambda_S}, \quad xq \sim A_q x^{-\lambda_g}$$
 (1)

with  $\lambda_S = \lambda_g$ . Unfortunately HERA is unable to measure  $F_2$  in this region of x and  $Q^2$ ; the reach of the collider is kinematically limited to the domain  $x/Q^2 \gtrsim 10^{-5} \,\text{GeV}^{-2}$ . Nevertheless as the precision of the HERA data improves it will be possible to determine  $\lambda_S$  and  $\lambda_g$  independently (see [7]). The sensitivity of the predictions to the interplay between the form of the gluon and the value of  $\alpha_S$  demonstrates the importance of a global analysis which includes the crucial large x constraints on  $\alpha_S$ . The  $\chi^2$  profiles shown in Fig. 1 that are obtained from the HERA data overconstrain  $\alpha_S$  since they are based on fits which set  $\lambda_S = \lambda_g$ . In our global " $\alpha_S$ " analysis this has a negligible effect on the partons, except at small x, where for  $Q^2$  values away from the HERA data there will be more variation than the spread that our curves imply.

The lower plot in Fig. 2 shows a typical set of the high precision BCDMS data [14]. In the large x domain these data place tight constraints on  $\alpha_S$ , free from the ambiguity associated with the gluon.

Fig. 3 gives another view of the constraints on the partons in various regions of x and  $Q^2$ . It is a contour plot of the ratio R of  $F_2$  as predicted by two sets of partons with  $\alpha_S(M_Z^2)$  fixed either side of the optimum value. In  $(x, Q^2)$  regions of precise data, acceptable fits demand that the ratio R be equal to 1. This is strikingly borne out. We see that the R=1 contour lies precisely in the centre of the band of the fixed-target deep inelastic scattering data. Again  $R \simeq 1$  in the region of the more accurate HERA data, that is  $x \lesssim 10^{-3}$  and  $Q^2 \sim 15 \text{ GeV}^2$ . When the precision of the HERA data improves and the accuracy extends over a larger domain of x and  $Q^2$  we would expect the  $R \simeq 1$  contour to also track the HERA band, but probably at the expense of allowing  $\lambda_S$  and  $\lambda_g$  to be free independent parameters. Of course Fig. 3 is just an overview of the description of one observable ( $F_2^{ep} = F_2^{\mu p}$ ). The global fit has many other constraints to satisfy. Nevertheless  $F_2^{ep}$  is measured over far wider regions of x and  $Q^2$  than the other observables and so Fig. 3 gives a useful indication of features of the global fit.

Additional experimental data in regions where the contours in Fig. 3 are closely spaced would clearly have significant impact on the analysis. For example sufficiently precise information in the region of high x and low  $Q^2$  (the lower left corner of Fig. 3) would help pin down  $\alpha_S$  even further. This is the domain of the SLAC experiments [20]. However we must take care to avoid regions where there are appreciable target-mass/higher-twist effects. For the SLAC data these effects are smallest in the region  $x \sim 0.3$ , provided that  $Q^2 \gtrsim 5 \text{ GeV}^2$  [1, 21, 22]. The Table below shows the  $\chi^2$  values for the subset of the SLAC data [20] that lie in the "safe" region  $(0.18 \lesssim x \lesssim 0.45)$  obtained from our sets of partons with different  $\alpha_S$ :

$\alpha_S(M_Z^2)$	0.105	0.110	0.115	0.120	0.125	0.130
$\chi^2(25 \text{ pts})$	37	24	25	46	93	179

The SLAC data clearly support the optimum value of  $\alpha_S$  determined by the other deep inelastic data, that is  $\alpha_S = 0.113$ . The inclusion of the SLAC data in the global fits would simply mean that the curves at x = 0.35, for example, would cross-over at a value just below the  $Q^2 = 50 \text{ GeV}^2$  intersection shown in Fig. 2.

Returning to Fig. 3 we see that jet production at large  $E_T$  at Fermilab samples partons in an  $x, Q^2$  domain far removed from the regions where deep inelastic measurements exist. For example, jets produced centrally with a transverse energy  $E_T = 300$  GeV sample  $x = 2E_T/\sqrt{s} \sim 0.3$  and  $Q^2 \sim E_T^2$ . Fig. 4 compares the observed single-jet inclusive distribution of CDF [23] with the predictions from partons with three different values of  $\alpha_S$ . For simplicity we have evaluated the leading-order expression at a common renormalization and factorization scale  $\mu = E_T/2$ . Of course a precision comparison between data and theory will require a full next-to-leading order analysis [24]. However, our aim here is to compare the spread of the predictions with the uncertainty of the data. A leading-order calculation is entirely sufficient for this purpose. A change of scale simply boosts the predictions up or down relative to the data, but leaves the shapes in Fig. 4 essentially unchanged. To consider the implications for partons it is necessary to discuss the description in two distinct regions of  $E_T$ . For  $E_T \lesssim 200$  GeV the jet cross section is dominated by the gg and gg initiated subprocesses. Here the cross section ratios reflect the different shapes of the gluon distributions in the region  $0.05 \lesssim x \lesssim 0.2$ , with the predictions spread out even more by the differences in the associated values of  $\alpha_S^2$ .

For  $E_T \gtrsim 200$  GeV, on the other hand, the cross section becomes increasingly dominated by quark-initiated subprocesses. Here the differences between the curves reflect the spread in the predictions of  $F_2$  at large x ( $x \gtrsim 0.25$ ) and large  $Q^2$  ( $Q^2 \sim E_T^2$ ), but now suppressed (rather than enhanced) by the differences in  $\alpha_S^2(Q^2)$ . This illustrative exercise demonstrates the value of a precise measurement of the jet distribution. If the experimental uncertainties can be reduced then these data will impose valuable constraints on the gluons at small x ( $x \sim 0.1$ ) and on the quarks at large x ( $x \sim 0.35$ ), as well as on the value of  $\alpha_S$ .

In summary we note that deep inelastic scattering data determine  $\alpha_S$  to be  $0.113 \pm 0.005$ . This value is found in an analysis of the BCDMS and SLAC data by Milsztajn and Virchaux [1] and in the global analyses [3, 7] which include, besides the BCDMS measurements, other deep inelastic and related data. Moreover the SLAC deep inelastic data [20], which are not included in the global fit, also favour this value of  $\alpha_S$ , see the Table above and the sample data in Fig. 2. The deep inelastic determination of  $\alpha_S$  relies mainly on the scaling violations of the data in the large x domain  $(x \gtrsim 0.2)$ , a region free from the gluon and its ambiguities. It is easy to verify that the low x HERA deep inelastic data for  $F_2^{ep}$  do not determine  $\alpha_S$  unless restrictive assumptions about the small x behaviour of the gluon and sea quark distributions are made. Indeed we find that the HERA data give little constraint on  $\alpha_S$  even with the assumption that  $\lambda_S = \lambda_g$  in (1). The values of  $\alpha_S$  determined from other (non deep-inelastic) processes cover a wider interval:  $0.110 \lesssim \alpha_S \lesssim 0.125$  [4]. Some methods rely on input partons and so there is a need for parton sets with values of  $\alpha_S$  which cover this interval. We have therefore performed a series of global analyses of the deep inelastic data to obtain realistic sets of partons corresponding to a sequence of values of  $\alpha_S(M_Z^2)$ . Since  $\alpha_S$  is not optimal these are compromise fits, which yield curves that intersect in the  $x, Q^2$  regions where precise data exist; see, for example, Fig. 2. The body of the deep inelastic data occurs in the region  $Q^2 \simeq 20 \; {\rm GeV^2}$ . Fig. 5 shows the gluon and up quark distributions from 3 parton sets with different  $\alpha_S$  for  $Q^2$ values above and below this value. The systematics displayed in these plots may be anticipated from Fig. 2. For low  $Q^2$ , below the body of the data, we see from Fig. 5(a) that the lower  $\alpha_S$ partons "swing more about the  $x \sim 0.05 - 0.1$  pivot points in favour of lower x"; and vice-versa for the high  $Q^2$  partons of Fig. 5(b). It is interesting to note that W and Z boson production at the Fermilab  $p\bar{p}$  collider sample u and d partons with  $x \sim 0.05$  and  $Q^2 \sim 10^4$  GeV<sup>2</sup>, that is in the region of the pivot point. The predicted production cross sections are therefore unusually stable to the change of the set of partons used in the calculation<sup>4</sup>. Jet production, on the other hand, samples partons over a range of x and  $Q^2$ , as well as being directly dependent on  $\alpha_S(Q^2)$ . It is therefore important to have to hand sets of realistic partons with different  $\alpha_S(M_Z^2)$ .

### Acknowledgements

We thank Nigel Glover for useful discussions and Joel Feltesse, Mark Lancaster and Anwar Bhatti for information concerning the data.

<sup>&</sup>lt;sup>4</sup>In particular we find that there is only a spread of  $\pm 3\%$  between the W cross section predictions obtained from our parton sets with  $\alpha_S = 0.115 \pm 0.010$ , which is well below the present experimental uncertainty, see, for example, ref. [3].

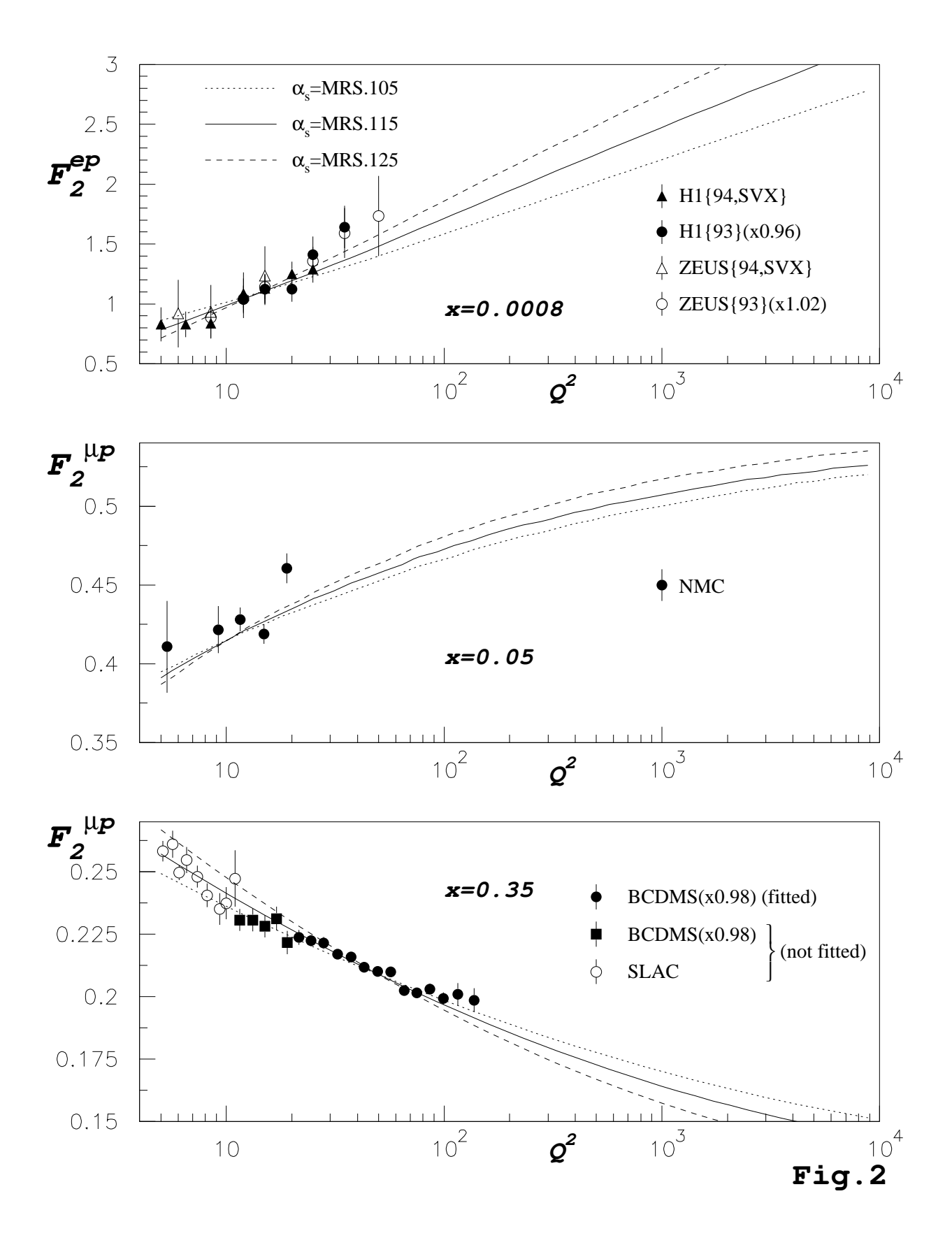
#### References

- [1] A. Milsztajn and M. Virchaux, Phys. Lett. **B274** (1992) 221.
- [2] CCFR collaboration: P. Z. Quintas et al., Phys. Rev. Lett. 71 (1993) 1307.
- [3] A. D. Martin, R. G. Roberts and W. J. Stirling, Phys. Rev. **D50** (1994) 6734.
- [4] B. R. Webber, Proc. of 27th Int. Conf. on H.E. Physics, Glasgow, 1994, eds. P. J. Bussey and I. G. Knowles (IoP publishing, 1995) p.213.
- [5] DIS + jet; H1 collaboration: T. Ahmed et al., Phys. Lett. B346 (1995) 415; G. Grindhammer, contribution to the Paris DIS 95 Workshop (April 1995).
   ZEUS collaboration: B. Foster, contribution to the Paris DIS 95 Workshop (April 1995).
- [6] D0 collaboration: S. Abachi et al., FERMILAB-Pub-95/085-E (W + jet).
- [7] A. D. Martin, R. G. Roberts and W. J. Stirling, Durham preprint DTP/95/14, to be published in Phys. Lett.
- [8] A. D. Martin, R. G. Roberts and W. J. Stirling, Phys. Rev. **D43** (1991) 3648.
- [9] CTEQ collaboration: H. L. Lai et al., Phys. Rev. **D51** (1995) 4763.
- [10] A. Vogt, DESY preprint 95-068 (1995).
- [11] M. Glück, E. Reya and A. Vogt, DESY preprint 94-206 (1994).
- [12] H1 collaboration: T. Ahmed et al., Nucl. Phys. **B439** (1995) 471.
- [13] ZEUS collaboration: M. Derrick et al., Z. Phys. C65 (1995) 379.
- [14] BCDMS collaboration: A. C. Benvenuti et al., Phys. Lett. B223 (1989) 485.
- [15] CCFR collaboration: S. R. Mishra et al., NEVIS preprint 1465 (1992).
- [16] NM Collaboration: P. Amaudruz et al., Phys. Lett. **B295** (1992) 159; Nucl. Phys. **B371** (1992) 3.
- [17] WA70 collaboration: M. Bonesini et al., Z. Phys. C38 (1988) 371.
- [18] ZEUS collaboration: contributions to the Paris DIS 95 Workshop (April 1995) by B. Foster and M. Lancaster.
- [19] H1 collaboration: contributions to the Paris DIS 95 Workshop (April 1995) by J. Dainton and G. Raedel.
- [20] L. W. Whitlow et al., Phys. Lett. **B282** (1992) 475.
   L. W. Whitlow, SLAC Report No. 357 (1990).

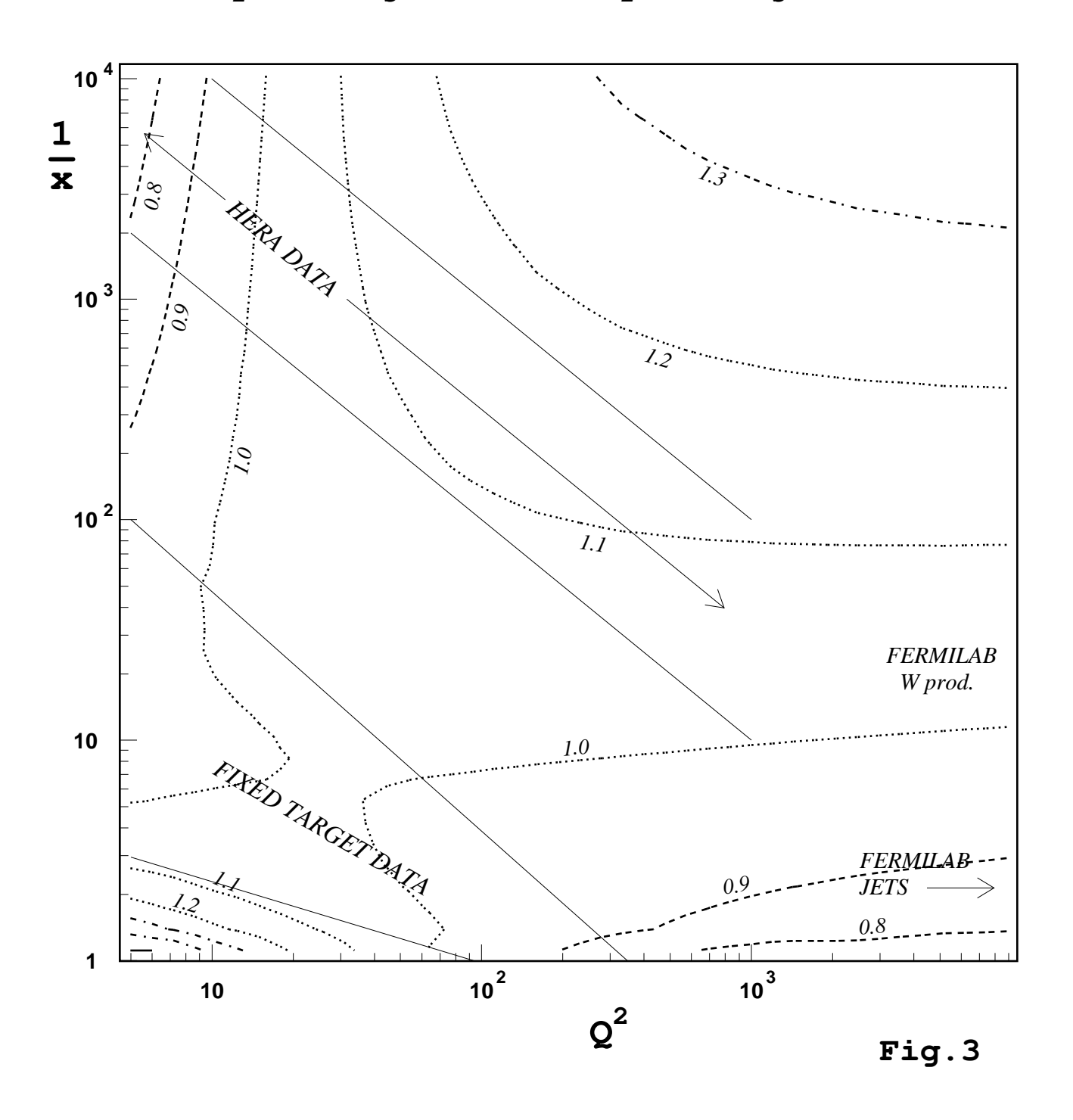
- [21] A. Milsztajn and M. Virchaux, Proc. of 32nd. Schladming Winter School, Austria 1993, eds. L. Mathelitsch and W. Plessas (Springer-Verlag, 1994) p.257.
- [22] A. D. Martin, R. G. Roberts and W. J. Stirling, Phys. Rev. **D51** (1995) 4756.
- [23] CDF collaboration: A. A. Bhatti, 10th Topical Workshop on proton-antiproton Collider Physics, Fermilab, May 1995.
- [24] S. D. Ellis, Z. Kunszt and D. E. Soper, Phys. Rev. Lett. 64 (1990) 2121.
  W. T. Giele, E. W. N. Glover and D. A. Kosower, Nucl. Phys. B403 (1993) 633.

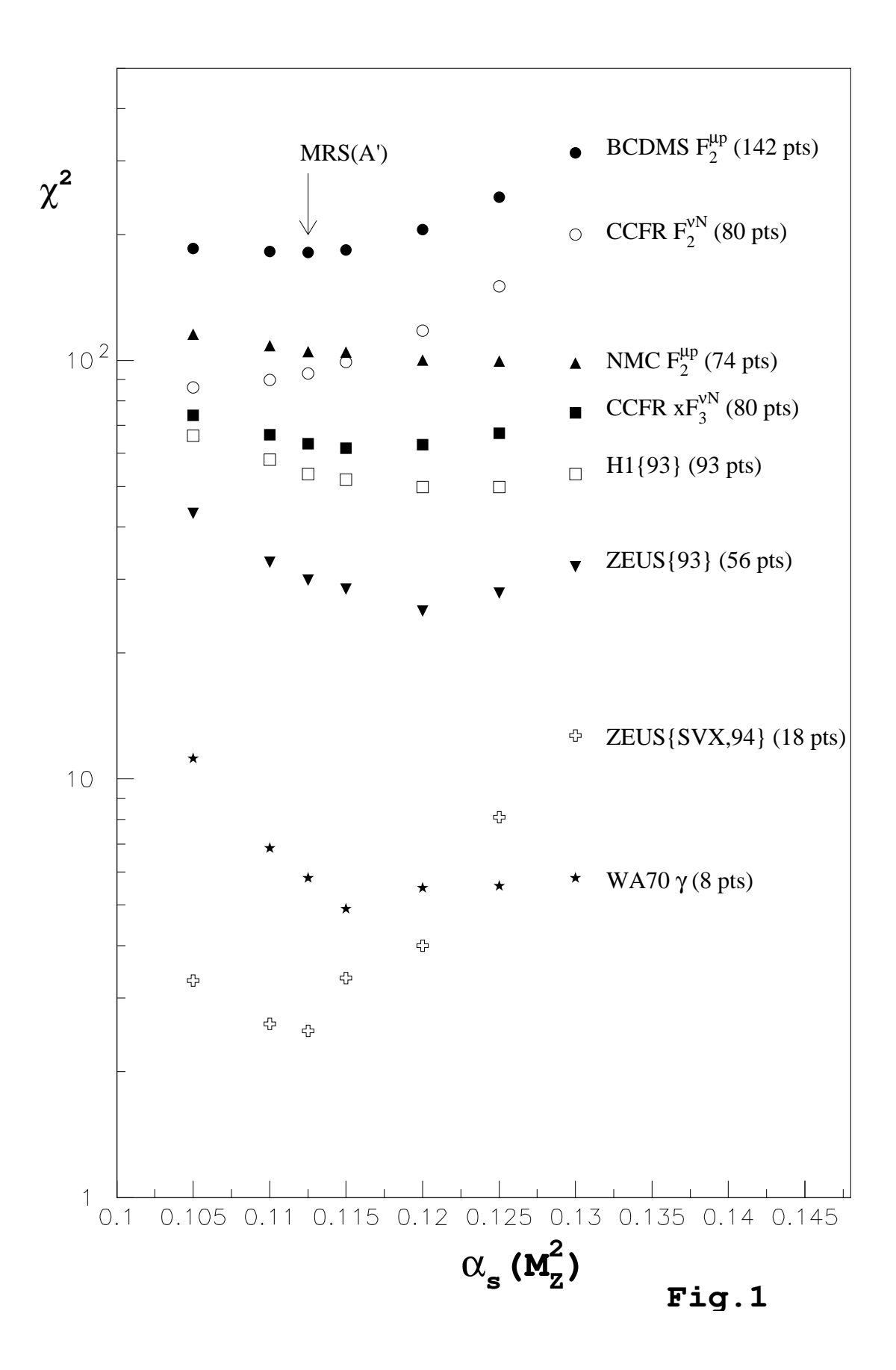
#### **Figure Captions**

- Fig. 1 The  $\chi^2$  values versus the value of  $\alpha_S$  used in the global analysis. The contributions to  $\chi^2$  are shown for the BCDMS [14], CCFR [15], NMC [16], WA70 [17], H1 (1993) [12] and ZEUS (1993) [13] data sets. The  $\chi^2$  values for the preliminary ZEUS (SVX) 1994 [18] data are also shown, but these data are *not* included in the fit. The  $\chi^2$  values are also shown for the MRS(A') set of partons [7], which has the optimum value of  $\alpha_S$ , namely  $\alpha_S = 0.113$ .
- Fig. 2 The scaling violations of  $F_2^{ep} = F_2^{\mu p}$  at three different values of x. The data are from refs. [14, 16, 12, 13, 18, 19]. The curves correspond to the global parton fits with  $\alpha_S = 0.105, 0.115$  and 0.125. At x = 0.35 some data points not normally included in our global fits are also shown: first, the lower  $Q^2$  BCDMS measurements which are made only at their lower beam energy and, second, SLAC data [20] in the region which is insensitive to target-mass/higher-twist corrections.
- Fig. 3 Contours of fixed  $R \equiv F_2^{ep}(\alpha_S = 0.125)/F_2^{ep}(\alpha_S = 0.105)$  in the  $x, Q^2$  plane, where  $F_2^{ep}(\alpha_S)$  is the structure function calculated from partons obtained in a global analysis with  $\alpha_S$  fixed at the given value. The bands indicate the regions where measurements of  $F_2$  exist. The HERA data are much more precise towards the low  $Q^2$  end of the band.
- Fig. 4 The  $p\bar{p}$ -initiated jet  $E_T$  distribution at  $\sqrt{s}=1.8$  TeV normalized to the prediction from partons with  $\alpha_S=0.115$  (i.e. MRS.115). The data are the CDF measurements of  $d^2\sigma/dE_Td\eta$  averaged over the rapidity interval  $0.1<|\eta|<0.7$  [23]. The curves are obtained from a leading-order calculation evaluated at  $\eta=0.4$ . The data are preliminary and only the statistical errors are shown. The systematic errors are approximately 25% and are correlated between different  $E_T$  points. We thank the CDF collaboration for permission to show these data.
- Fig. 5 The xg and xu parton distributions at (a)  $Q^2 = 5 \text{ GeV}^2$  and (b)  $Q^2 = 10^4 \text{ GeV}^2$  of the parton sets with  $\alpha_S = 0.105, 0.115$  and 0.125.



# $F_2(x, Q^2, \alpha_s = 0.125) / F_2(x, Q^2, \alpha_s = 0.105)$





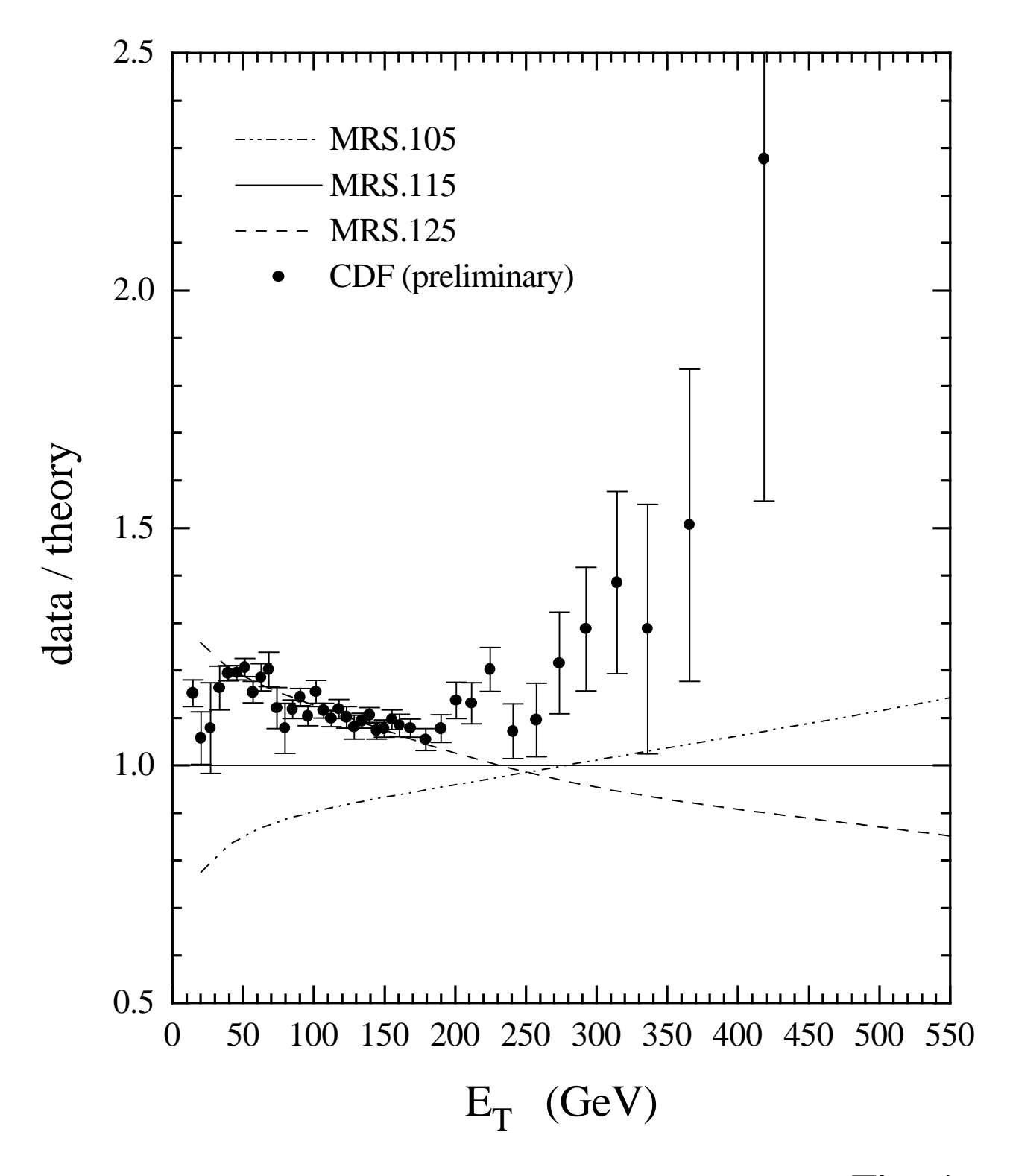


Fig. 4

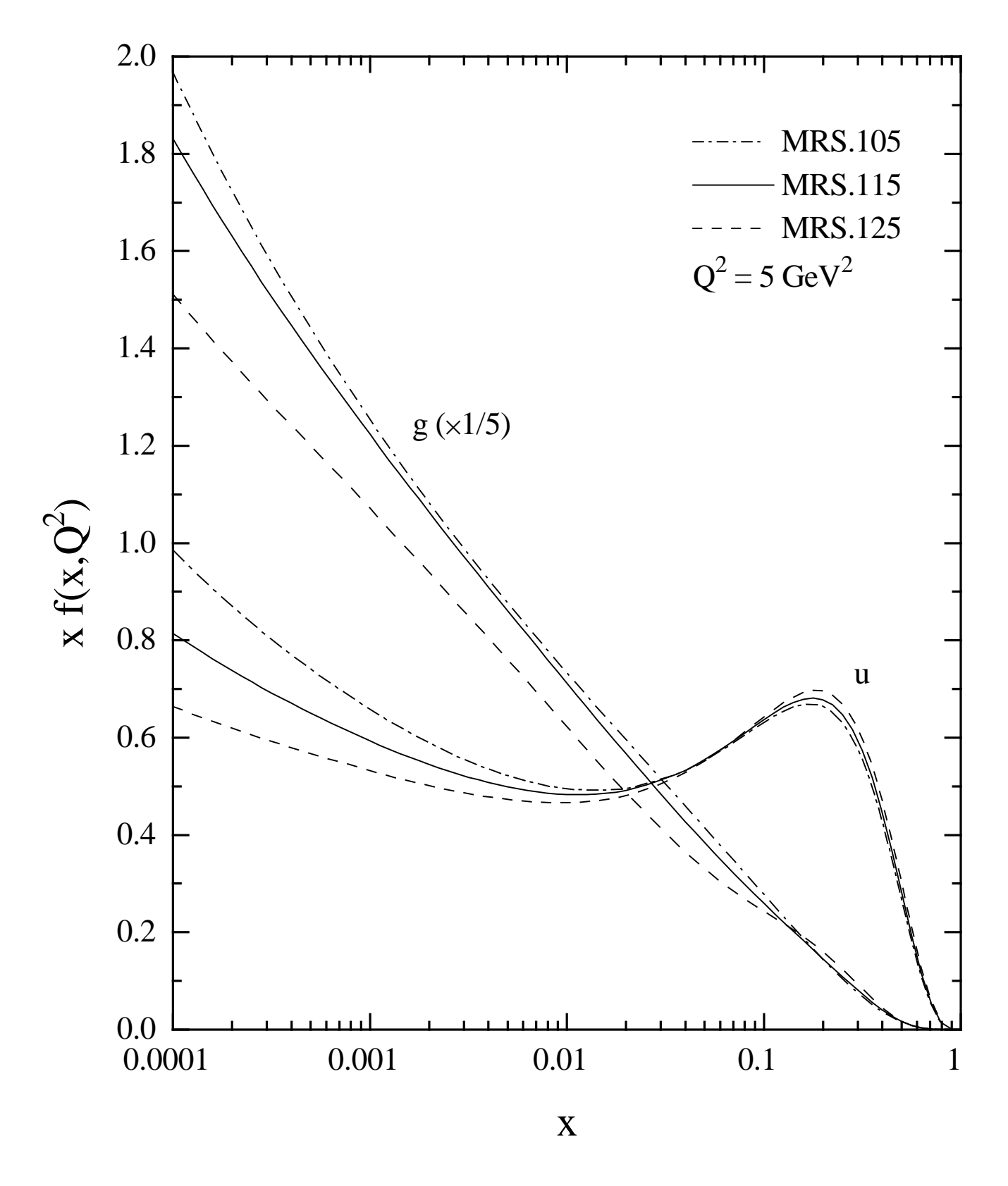


Fig. 5(a)

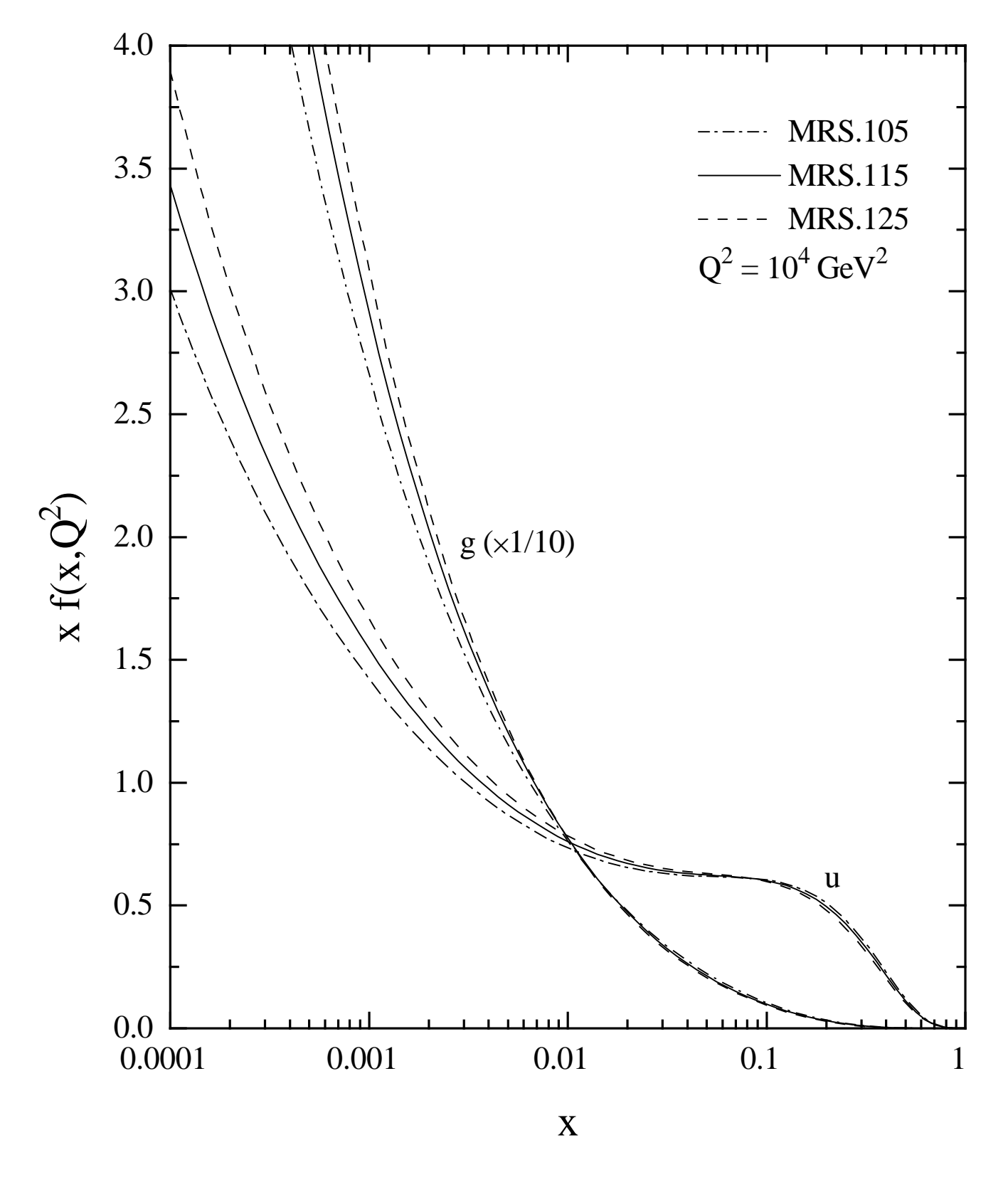


Fig. 5(b)